Polarization charge screening and indium surface segregation in (In,Ga)N/GaN single and multiple quantum wells

O. Mayrock,* H.-J. Wünsche, and F. Henneberger
Humboldt-Universität zu Berlin, Institut für Physik, Photonik, Invalidenstrasse 110, D-10115 Berlin, Germany
(Received 13 April 2000)

Energies and oscillator strengths of the optical transitions in (In,Ga)N/GaN quantum-well structures with thin cap layers are investigated theoretically. Based on a self-consistent solution of the Schrödinger-Poisson equations, the internal fields generated by spontaneous surface charges and piezoelectric interface charges are systematically discussed for different sample configurations under consideration of indium surface segregation. We vary background doping density, thickness of the cap layer, number of quantum wells, indium content, and polarity of the structure. Indium surface segregation is shown to result in a blueshift of the transition energy and in a decreased optical matrix element at the same time. Background doping influences the band-edge alignment not only via screening of the polarization charge at the material interfaces by quantum-confined carriers, but also via ionized dopants in depletion layers. This becomes particularly important in case of Ga-face-grown material with *n*-type doping. We find that the position of the quantum well within the sample severely affects transition energy and optical matrix element.

I. INTRODUCTION

(In,Ga)N attracted much interest in the last few years since it has become the key material in commercial fabrication of long-lifetime light-emitting diodes (LED's) and laser diodes (LD's) for the blue to ultraviolet spectral range. Up to now, exclusively (In,Ga)N is used as active region in these devices. However, the light-emitting mechanism is not yet fully understood because this material system exhibits some peculiarities.

The rather poor structural material quality in terms of defect density, compositional homogeneity, abrupt interfaces, etc. compared to other heterostructures is mainly a consequence of a strong chemical difference between GaN and InN. It results in (i) a broad solid phase miscibility gap[1] between GaN and InN, giving rise to phase separation, and (ii) a large lattice mismatch between well and barrier material associated with a high dislocation density. Much effort has been made to investigate spatial extension and depth of compositional fluctuations[2,3] as well as their impact on the optical properties. The huge Stokes shift of the emission line has been attributed to carrier localization in band-tail states.[4]

Another peculiarity results from the polar axis of the wurtzite crystal structure and the strong polarity of the III-N bindings. All group-III nitrides in the wurtzite phase have a strong spontaneous macroscopic polarization and large piezoelectric coefficients. This has been found from *ab initio* calculations.[5,6] The abrupt variation of the polarization at surfaces and interfaces gives rise to large polarization sheet charges that in turn create internal electric fields of the order of MV/cm. A huge redshift of the transition energy and a strong increase of the carrier lifetime due to the quantum-confined Stark effect are marked features in the optical spectra of (In,Ga)N/GaN quantum wells, extensively debated in many publications.[7–13] First estimates were restricted to the bare field profiles for single and multiple quantum wells (SQW's and MQW's) in undoped material. They yielded a qualitative understanding of the spectra.[7–10] More elaborate self-consistent calculations of the Schrödinger and Poisson equations allowed one to explain shifts of transition energy and modifications of carrier lifetime by screening of polarization charges and potential fluctuations in highly doped samples or under high excitation.[11,14–17]

In this paper, we give a detailed description and analysis of the overall electric-field situation along the growth direction in (In,Ga)N/GaN SQW's and MQW's. We focus on a sample design with a thin cap layer, typical of excitation experiments. In this situation, both the spontaneous surface polarization charge of the cap and the piezoelectric interface polarization charges of the wells influence the band-edge alignment, and thus optical transition energies and matrix elements. Previous calculations reported in the literature up to now treated only the case where QW's are decoupled from the sample surface,[11,14–16] or MQW's in a *p-n* junction and transistor structures.[17] Our results demonstrate that optical transition energies and matrix elements depend sensitively on the design of the structure.

Furthermore, we investigate for the first time the combined impact of polarization fields and indium surface segregation. A strong tendency of indium surface segregation during the growth of (In,Ga)N can be expected as a consequence of the large difference between the free binding enthalpies of GaN and InN.[3,18–20] This effect is well investigated for comparable arsenide heterostructures.[21–25] Segregation limits the indium incorporation and smoothes the structural transitions between well and barrier materials. Hence it redistributes the polarization charge into a wider space region, so that the resultant electric field may be much different from that for ideal interfaces.

We present a self-consistent treatment of Poisson and Schrödinger equation for various experimentally relevant geometries of (In,Ga)N/GaN SQW's and MQW's. For the (In,Ga)N well material, the homogeneous alloy model is adopted. This simplifying assumption appears to be justified in our case since the macroscopic redistribution of charge

due to the screening of polarization fields in a QW stack is not much affected by compositional inhomogeneities in the wells. Furthermore, several characteristic experimental findings like the dependence of the emission energy on the well width[8,26] (*quantum-confined Stark effect*) and the emission energy shift induced by injection current[11] or by photoinduced excitation density[15] could be explained with this approximation.

The paper is organized as follows. The theoretical model and the range of parameters are given in Sec. II. The results of the self-consistent calculations for different segregation profiles of an otherwise fixed SQW are discussed in Sec. III. Section IV follows with a detailed analysis of the electric-field situation of SQW's and MQW's with a fixed representative segregation profile for various experimentally relevant geometries. We discuss the different physical situations with an emphasis on the screening of polarization fields. To allow simple estimates for a given sample, analytical approximations are derived for the field profile in all cases. The paper is summarized in Sec. V.

II. THEORY

We consider wurtzite $In_xGa_{1-x}N$/GaN SQW's and MQW's with a thickness of $d=3$ nm, as widely used in LED's and LD's. The growth axis is the crystallographic c axis. The QW's are assumed to be pseudomorphically grown on a relaxed GaN buffer and capped with a GaN layer. Three representative indium concentrations $x=0.05$, 0.1, and 0.2 will be compared. A constant donor concentration N_D throughout all layers is assumed. The cases of low, medium, and high doping are considered, represented by $N_D=5\times10^{16}$, 5×10^{17}, and 5×10^{18} cm^{-3}, respectively.

The band-edge energy discontinuities at heterointerfaces can be expressed as

$$E_a(x)=\xi_a E_g(x) \quad (a=e,h), \tag{1}$$

where $\xi_e=\Delta E_e/\Delta E_g$ and $\xi_h=\Delta E_h/\Delta E_g=1-\xi_e$ are the relative band offsets in the conduction and valence bands, respectively. For the dependence of the band-gap energy E_g of strained $In_xGa_{1-x}N$ on x, we use the common interpolation

$$E_g(x)=E_g^{GaN}(1-x)+E_g^{InN}x-bx(1-x). \tag{2}$$

The bowing parameter b phenomenologically accounts for the nonlinearity of the relation. The material parameters used in the calculation are listed in Table I.

The polarization in wurtzite nitrides is oriented along the c axis. The total polarization of $In_xGa_{1-x}N$ can be written as a function of the indium content,[5,7]

$$P(x)=e_{33}\epsilon_\perp(x)+2e_{31}\epsilon_{||}(x)+P_{sp}(x), \tag{3}$$

where the first two terms describe the strain-induced (piezoelectric) part, oriented in the [0001] direction [according to the compressive strain state of (In,Ga)N pseudomorphically grown on relaxed GaN]. The spontaneous contribution $P_{sp}(x)$ points in the $[000\bar{1}]$ direction. e_{ij} are the coefficients of the piezoelectric tensor, and

TABLE I. Calculation parameters. The abbreviation lin. int. stands for linear interpolation.

Parameter	GaN	InN	(In,Ga)N
a (nm)[a]	0.3189	0.354	lin. int.
c (nm)[a]	0.5185	0.570	lin. int.
E_g (eV)[b]	3.4	1.8	
b (bowing) (eV)[c,b]			2.5
m_e/m_o[d,b]	0.2	0.2	
m_h/m_o[e,b]	1.0	1.0	
ε[b]	9.5	12.0	lin. int.
T (K)	300	300	
$\Delta E_C/\Delta E_V$[f]			70/30
P_{sp} (C/m^2)[g]	−0.029	−0.032	lin. int.
e_{33} (C/m^2)[g]	0.73	0.97	lin. int.
e_{31} (C/m^2)[g]	−0.49	−0.57	lin. int.
C_{11} (GPa)[h]	367	223	lin. int.
C_{12} (GPa)[h]	135	115	lin. int.
C_{13} (GPa)[h]	103	92	lin. int.
C_{33} (GPa)[h]	405	224	lin. int.

[a]Reference 27.
[b]These numbers are typical values within the according spectrum given in literature. The choice of these parameters is not critical concerning the qualitative results of our calculation.
[c]Reference 28.
[d]Reference 29.
[e]References 29 and 30.
[f]Reference 31.
[g]Reference 5.
[h]Reference 32.

$$\epsilon_{||}(x)=\frac{a_{GaN}-a(x)}{a(x)} \quad \text{and} \quad \epsilon_\perp(x)=\frac{\tilde{c}(x)-c(x)}{c(x)} \tag{4}$$

are the strain components parallel and perpendicular to the QW plane, respectively. The corresponding lattice constants are denoted a and c. Vegard's law is assumed for calculating the relaxed lattice constants $a(x)$ and $c(x)$ of the ternary (In,Ga)N alloy. The actual lattice constant $\tilde{c}(x)$ of the strained (In,Ga)N QW is determined by the elastic constants C_{ij} of the material

$$\tilde{c}(x)=c(x)\left(1-2\frac{C_{13}}{C_{33}}\epsilon_{||}(x)\right). \tag{5}$$

Two possible orientations of the spontaneous polarization with respect to the growth direction have to be distinguished. The polarization vector points toward the substrate in case of Ga-face polarity and toward the surface in case of N-face polarity.[33] Both polarization types can be grown, and will be compared in the following. The orientation of the z axis is always chosen along the spontaneous polarization, i.e., in the $[000\bar{1}]$ direction.

$P[x(z)]$ varies with the vertical coordinate z via the variation of the indium content, and hence exhibits discontinuities at the respective interfaces. These spatial variations of P give rise to the polarization charge density

$$\rho_{pol}(z) = -\frac{\partial}{\partial z} P[x(z)], \tag{6}$$

that in turn creates huge electric fields. The abrupt disappearance of the spontaneous polarization P_{sp} at the surface causes a bare field as large as $|F_{sp}| = |P_{sp}/\varepsilon\varepsilon_0| \approx 3.5$ MV/cm. Inside the QW, the piezoelectric contribution dominates the polarization, because the spontaneous polarizations of GaN and InN do not differ noticeably. It is oriented opposite to the spontaneous polarization, and the corresponding bare piezoelectric fields range between 0.85 and 3.5 MV/cm for the investigated compositions.

The mutual interaction of these fields and occupied electronic states can be described by the Schrödinger–Poisson system of equations. The energies ε_a^k and wave functions $\psi_a^k(z)$ of the electron and hole subbands are determined from the single-particle effective-mass Schrödinger equations

$$\left[-\frac{\hbar^2}{2m_a}\frac{\partial^2}{\partial z^2} + V_a(z) \right] \psi_a^k(z) = \varepsilon_a^k \psi_a^k(z), \quad a = e,h, \tag{7}$$

with the potentials

$$V_a(z) = E_a(z) + q_a\phi(z). \tag{8}$$

k labels the subbands. $E_a(z)$ are the band-edge discontinuities according to Eq. (1), the second term is the electrostatic contribution. $q_e = -e$ and $q_h = +e$ denote the electron and hole charges, respectively. All charge densities of the system act as sources of the electrostatic potential $\phi(z)$ according to the Poisson equation

$$\frac{\partial^2}{\partial z^2}\phi(z) = -\frac{e[n_h(z) - n_e(z) + N_D] + \rho_{pol}(z)}{\varepsilon\varepsilon_0}. \tag{9}$$

The particle densities herein are given by

$$n_a(z) = N_a \sum_k |\psi_a^k(z)|^2 \ln(1 + e^{(F-\varepsilon_a^k)/kT}), \tag{10}$$

where F is the Fermi energy and $N_a = m_a kT/\pi\hbar^2$ is an effective two-dimensional density of states. $T = 300$ K is used in all calculations presented below, corresponding to device applications at room temperature. We have redone some calculations for lower temperatures. Although the distribution of carriers among the subbands changed noticeably, the total sheet densities in the QW's was less sensitive, and the global field profile changed only slightly.

Because the densities depend in turn on the subband energies and wave functions, the basic equations (7)–(10) become coupled and have to be solved self-consistently. This calculation was performed iteratively, using the numerical method of finite differences.[34,35] The polarization charges were simulated by additional, fully ionized dopants, discretized in 1-Å-wide steps on the numerical space grid. The Schrödinger equation is solved only in a limited region that includes the cap layer, the QW stack, and some ten nanometers of the buffer. Vanishing of the wave function ψ is used as boundary condition on both sides. The rest of the buffer layer is treated as a bulk material. There only the Poisson equation is solved with the expression

$$n_a(z) = N_a^{3d} \mathcal{F}_{1/2}\left(\frac{F - E_a - q_a\phi}{kT} \right) \tag{11}$$

for the particle densities on the right hand side. $\mathcal{F}_{1/2}$ is the Fermi integral with index 1/2 and $N_a^{3d} = 2(2\pi m_a kT/h^2)^{3/2}$. The buffer layer is assumed to be very thick compared with the heterostructure, so that the influence of the substrate interface is negligible.

During the self-consistency run only sufficiently occupied subbands are accounted for. However, to obtain optical transition energies and overlap integrals $\int dz\, \psi_e(z)\psi_h(z)$, unoccupied states have to be considered as well. Therefore, these additional subband energies and wave functions were calculated by a postprocessing procedure. Restricting ourselves to confined states only, the Schrödinger equation is solved for each QW separately using again the method of finite differences. This simulates only the situation of low excitation density, where the band-edge alignment is not altered by photoexcited carriers. Our calculation of the transition energy includes furthermore a perturbative correction due to exciton binding[36] for densities below the Mott transition, and due to the exchange contribution to the band-gap renormalization above the Mott transition. The Mott transition is assumed to occur when the band-gap renormalization is equal to the exciton binding energy.

III. INDIUM SURFACE SEGREGATION

Due to the large difference between the free binding enthalpies of GaN and InN,[18] indium surface segregation during the growth of (In,Ga)N can be expected.[3,19,20] As a result, the profile of incorporated indium is not rectangularly shaped, as usually assumed for calculating subband states and optical properties. However, it is rather difficult to measure the actual distribution of indium along the growth direction.[3] In most cases only the nominal integral indium content of one QW-barrier period, and the well and barrier thicknesses in a MQW are known from the growth process or from experiments like, e.g., x-ray-diffraction measurements. In this section, we discuss the consequences of nonrectangularly shaped indium profiles in the presence of polarization fields.

To mimic the indium profile, several suggestions have been made in literature,[3,21–23] most of them for arsenides.[21–23] We use error functions with segregation lengths L_{si} and L_{sn} for the inverted (InGaN-on-GaN) and normal (GaN-on-InGaN) interfaces, respectively,

$$x(z_i \pm \delta) = \begin{cases} 0, & \delta < 0 \\ x_o \,\mathrm{erf}\left(\dfrac{\delta}{L_{si}}\right), & 0 \leqslant \delta < d \\ x_o \,\mathrm{erf}\left(\dfrac{d}{L_{si}}\right)\left[1 - \mathrm{erf}\left(\dfrac{\delta - d}{L_{sn}}\right)\right], & d \leqslant \delta, \end{cases} \tag{12}$$

where z_i denotes the position of the inverted interface, and δ is the distance from z_i in the growth direction. Accordingly, the positive sign on the left side holds for N-face material and the negative one for Ga-face material, accounting for the

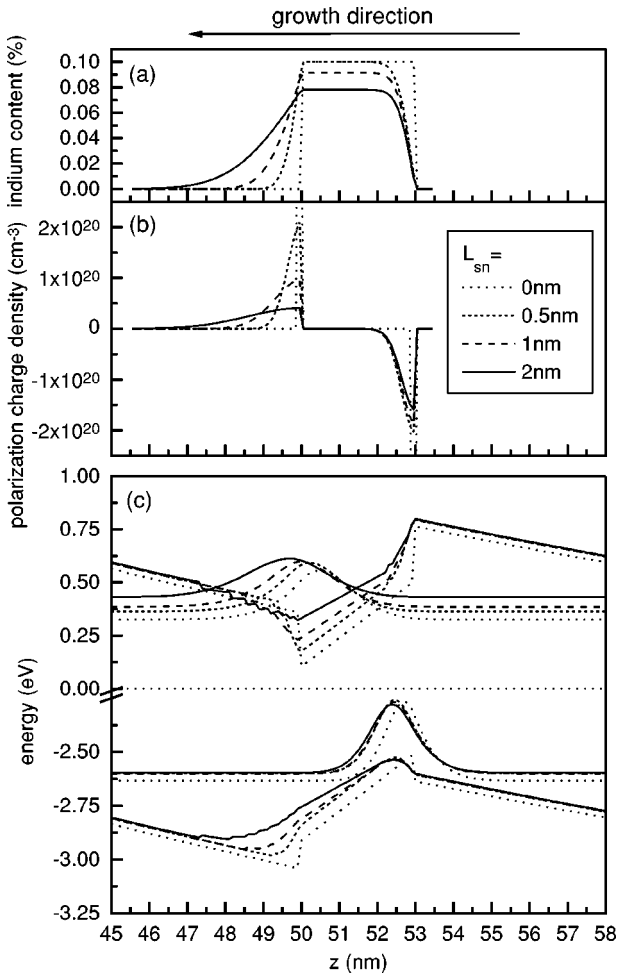

FIG. 1. (a) Indium profile, (b) polarization charge density, (c) self-consistently calculated band-edge alignments, and subband functions of a Ga-face grown 3-nm $In_{0.1}Ga_{0.9}N/GaN$ SQW with a background donor density of $N_D=5\times10^{17}$ cm^{-3}, and a 50-nm cap layer for different indium segregation profiles. The segregation length at the inverted interface is 0.5 nm, and that at the normal interface is varied as indicated in the legend.

different orientations of the z axis. The parameter x_0 is used to set the mean indium content $\int d\delta x(z_i\pm\delta)/d$ to the desired value.

There is experimental indication for an asymmetry of the segregation length at the two interfaces with respect to growth direction.[3] For arsenides, this is confirmed experimentally in several different ways,[22,23,25] and can be explained by a local equilibrium model for the growth process.[22] In general, the segregation length of the more weakly bound III component in ternary III-V compounds is known to be a function of growth parameters like the III-V ratio and the substrate temperature.[21–24] Since no values for L_{si} and L_{sn} for (In,Ga)N/GaN heterostructures are available from experiment, we tried to make a reasonable choice, keeping L_{si} at 0.5 nm and varying L_{sn} from 0.5 nm to 2 nm [see Fig. 1(a)]. The integral indium content was kept fixed. The calculation was executed for a $d=3$ nm SQW, scanning the whole range of parameters given in Sec. II. As an example, indium profiles (a), polarization charge densities (b), self-consistently calculated band edge profiles and subband functions (c) for a Ga-face grown SQW with $x=0.1$ and a 50-nm cap layer are displayed in Fig. 1.

In the case of weak and symmetric segregation ($L_{si}=L_{sn}<d$), the polarization field remains nearly unchanged [dotted and short-dashed lines in Fig. 1(c) are parallel inside the QW], and the transition energies are only slightly changed. A small blueshift as well as redshift can occur, depending on the specific set of parameters. Electron and hole wave functions are somewhat shifted in the growth direction, but the overlap is hardly modified.

A clear blueshift is obtained with increasing L_{sn}. It reaches about 30, 60, and 100 meV for compositions $x=0.05$, 0.1, and 0.2, respectively, in case of the largest segregation length $L_{sn}=2$ nm. This segregation-induced correction compensates for up to one-third of the corresponding quantum-confined Stark shift of 90, 210, and 470 meV, respectively, for the rectangular QW with $N_D=5\times10^{16}$ cm^{-3}. Two combined effects contribute to this behavior. First, the material gap within the QW increases because the indium profile becomes not only broader but also flatter in order to conserve the total amount of incorporated indium. Second, the flattening of the profile is accompanied by a reduction of the strain. Hence the amount of polarization charges at the interfaces drops down. This effect is clearly observable in Fig. 1(b) as a reduction of the amplitude of the charge-density profile at the inverted interface. As a consequence, the field strength in the QW decreases, reducing the quantum-confined Stark shift.

For ideal interfaces, a reduced polarization field would also raise the electron-hole overlap. Conversely, segregation results in a significant reduction of the overlap down to approximately a factor 0.2 for $x=0.2$. Although the spatial extensions of the subband functions increase in the present case, the overlap is reduced due to a counteracting increase of the separation between electrons and holes. Because of the asymmetry of the segregation lengths at the two interfaces, the shift of the electron wave function toward the surface is larger than the shift of the hole wave function [see Fig. 1(c)].

Concluding so far, the optical transitions are blueshifted with increasing indium surface segregation in the considered 3-nm-wide SQW's. This blueshift compensates for up to one-third of the redshift from the quantum-confined Stark effect. It is accompanied by a further reduction of the oscillator strength due to the asymmetry of the segregation lengths. In Sec. IV, we consider different positions of SQW and MQW structures. To keep the efforts limited, the further calculations are carried out with a fixed choice of $L_{si}=0.5$ nm for the inverted and $L_{sn}=1$ nm for the normal interface, representing a lower limit for the segregation.

IV. POLARIZATION CHARGE SCREENING

The electric field generated by the polarization charges ρ_{pol} is modified by fields caused by mobile carriers and dopant space charges according to Poisson equation (9). Therefore, the optical properties of a QW do not only depend on its local composition but also on the global distribution of polarization and screening charges. In this section, we study the screening situation for different types of heterostructures. Because group-III nitrides tend to exhibit *n*-type conductivity, we focus on this case.

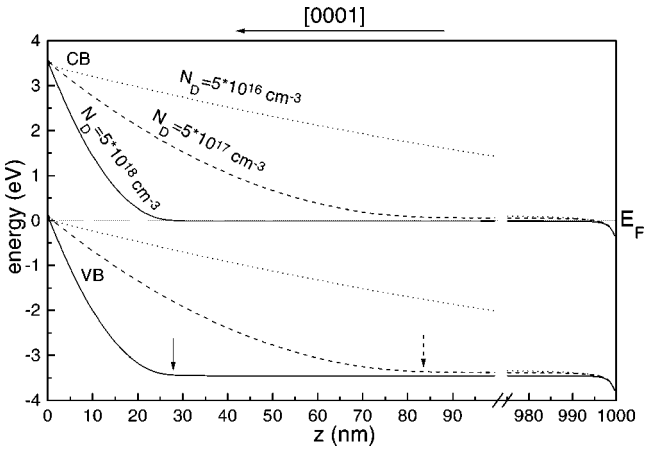

FIG. 2. Band-edge alignment along the *c* axis of a bare GaN layer for several background donor densities. The Ga face is at the origin of the abscissa, and has a negative polarization charge; the N face at the opposite side has a positive polarization charge. The arrows indicate the border of the depletion layer according to Eq. (14).

A. Homogeneous GaN slab

It is useful to start with the most simple case, a layer of homogeneous, unstrained GaN. Spontaneous polarization here causes surface charge densities of about ± 0.03 C/m^2. Without screening, these charges would cause a voltage drop across a 1-μm-thick layer as large as 350 V. However, it is well known[16] that screening by mobile carriers reduces this voltage down to approximately the gap voltage E_g/e. The self-consistently calculated band-edge alignments, displayed in Fig. 2, show this behavior for all considered doping concentrations. Three different types of screening charges appear.

(a) Close to the N face, the conduction band falls below the Fermi level. This is the signature of an electron accumulation layer shielding the positive polarization charge. Beyond this layer, which is only few nm wide, the field strength is practically zero.

(b) The valence-band edge lies above the Fermi level just at the Ga face. For the considered *n*-type material, this indicates an inversion layer. This layer is thinner than the electron accumulation layer at the N face due to the larger density of states in the valence band.

(c) The inversion layer screens the surface polarization charge not completely. The residual field drops to zero due to the space charge of the ionized impurities within an extended surface depletion layer.

Useful analytical approximations of some quantities can be found from device physics[37] when neglecting the finite width of the inversion layer and considering that the conduction band edge of the *n*-type GaN is practically at the Fermi level E_F. Then the band edges in the surface depletion layer vary quadratically:

$$E_e(z) = E_F + E_g\left(\frac{z}{w_s} - 1\right)^2. \tag{13}$$

The corresponding values for the width of the surface depletion layer,

$$w_s = \sqrt{\frac{2E_g\varepsilon\varepsilon_0}{e^2 N_D}}, \tag{14}$$

are indicated by arrows in Fig. 2. It can be seen that formula (14) gives a good approximation of the fully self-consistent calculation. The electric-field strength $F = -(\partial/\partial z)\phi$ in the surface depletion layer decreases approximately linearly with z to zero:

$$F(z) = -\frac{eN_D}{\varepsilon\varepsilon_0}(w_s - z). \tag{15}$$

The corresponding sheet charge density of the inversion layer at the Ga face is given by

$$\sigma_{inv} = P_{sp} - \sqrt{2E_g N_D \varepsilon\varepsilon_0}. \tag{16}$$

All these estimates hold as long as w_s remains smaller than the slab thickness D and the space charge $eN_D w_s$ is smaller than P_{sp}. For realistic dopings and thicknesses, this is always the case, and the top and bottom of the slab are decoupled by a field-free bulk layer. Therefore, the field situation on top of the slab is independent of the substrate properties. In the less realistic limit of a vanishing doping density, the surface depletion layer would fill the whole slab with a constant residual field $F = E_g/eD$. To summarize, a Ga-face-grown *n*-type sample will exhibit a combined hole inversion and depletion layer at the surface, whereas the polarization charges on top of a N-face-grown sample are screened by an electron accumulation layer.

Fermi-level pinning by gap states at the surface may modify the situation. In this case positively charged surface states take over the role of the inversion layer, E_g has to be replaced in the above considerations by $E_c - E_F$ at the surface, and the space-charge region becomes accordingly thinner. However, Fermi-level pinning requires that the density of these surface states is larger than the high number density of polarization charges of approximately 10^{13} cm^{-2}. Depending on the preparation of the samples, this may be the case, but there are not many investigations on this up to now.[38] Therefore, we do not consider this effect in the following.

B. Single quantum well

Now we consider a SQW with $d = 3$ nm, embedded in *n*-type GaN. In Ga-face-grown samples, the depletion layer can penetrate the QW and alter its properties. This is not the case in N-face-grown material. To investigate this effect, we compare N- and Ga-face-grown samples with two different cap layer thicknesses in each case. The results of the calculations for the four geometries are summarized for $x = 0.1$ in Fig. 3. In the following, the differences between these four geometries are discussed in detail.

1. N-face sample with thick cap

The band profile of a N-face-grown QW with a 50-nm cap layer in the high doping case $N_D = 5 \times 10^{18}$ cm^{-3} is given by the solid line at the right side of Fig. 3(c). Within some nm above the negatively charged interface of the QW, the conduction-band edge lies above the Fermi level. The electrons from this depletion layer have been transferred to the

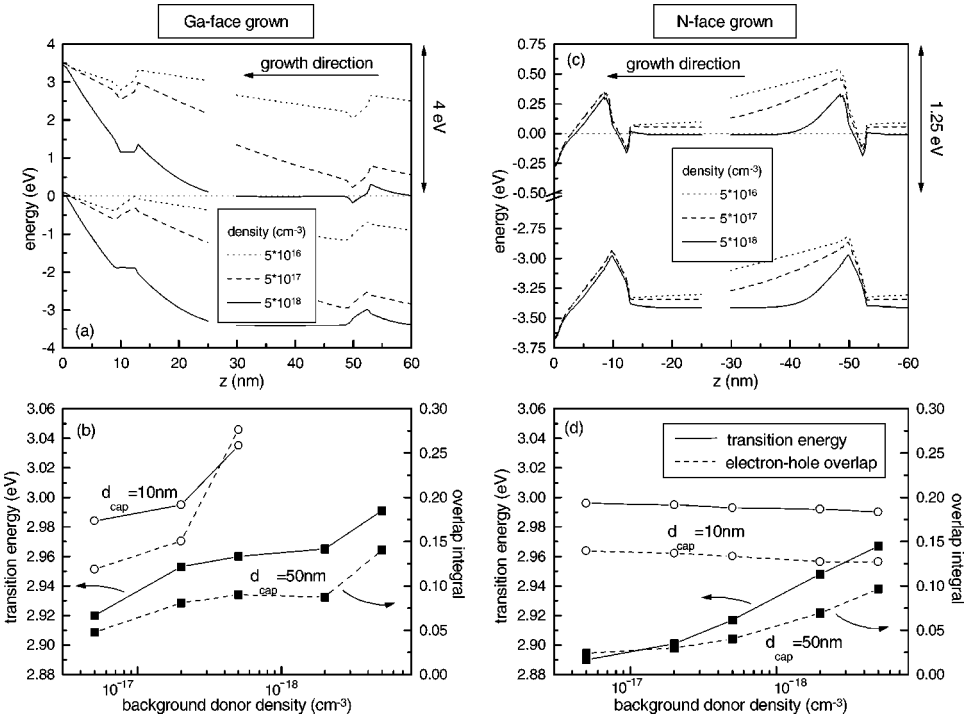

FIG. 3. (a) and (c) Self-consistently calculated band-edge alignments of a Ga-face-grown (a) and N-face-grown (c) 3-nm $In_{0.1}Ga_{0.9}N/GaN$ SQW's for various background donor densities and for 10- and 50-nm cap layers, respectively. The z axis is always oriented along the direction of the spontaneous polarization of relaxed GaN with the origin at the surface. The effect of indium surface segregation is included (see Sec. III). The surface is at the origin of the abscissa. (b) and (d) Transition energy and electron-hole overlap integral as functions of a homogeneous background donor density.

first electron subband in the QW, the band edge of which lies below the Fermi level. The voltage drop caused by the excess electrons in the QW and the space charges just compensates for the voltage drop $F_p \times d$ of the bare piezoelectric field F_p across the QW. As a consequence, the band edges become horizontal and equal to the bulk values on both sides sufficiently far from the QW. As long as this holds, the QW is not influenced by the surface, and has its *intrinsic configuration*.

It is useful to obtain analytical estimates for the relevant quantities characterizing this configuration. For this purpose we approximate the excess electrons in the lowest subband by a negative charge sheet located at the positive interface of the QW, assume an abrupt space-charge layer of width w, and again apply standard device physics.[37] Vanishing fields sufficiently far from the QW require $\sigma_e = -eN_D w$ for the sheet density of excess electrons. Furthermore, the voltage drop across all screening charges has to compensate for the voltage drop $F_p \times d$ of the bare polarization field across the QW. This yields

$$w = d\sqrt{\frac{2\sigma_p}{eN_D d}} \tag{17}$$

for the width of the depletion layer, measured from the positively charged interface of the QW. The field in this layer varies like

$$F(z) = -\frac{eN_D}{\varepsilon\varepsilon_0}(z_i + w - z) + F_p \Theta_{\mathrm{QW}}(z), \tag{18}$$

where z_i is the position of the positively charged inverted interface of the QW. The function $\Theta_{\mathrm{QW}}(z)$ is a projector to the well. It is equal to unity inside the QW, and vanishes outside.

The transition energies [Fig. 3(d)] exhibit a blueshift by about 80 meV when increasing the donor concentration from 5×10^{16} to 5×10^{18} cm^{-3}. 40- and 150-meV blueshifts are obtained for the alternative compositions $x=0.05$ and 0.2, respectively. The blueshift is accompanied by an increase of the electron-hole overlap [Fig. 3(d)]. This is the anticipated behavior, commonly attributed to the increased screening of the polarization fields. Figure 3(c) shows, however, that the reduction of the field is not sufficient for explaining the shift. In addition, the band-edge alignment in the space-charge layer of the barrier changes, which strongly increases the hole confinement energy. The combination of both effects is responsible for the total blueshift and the increase of the overlap.

2. N-face sample with thin cap

For the 10-nm cap layer, the space-charge layer in the barrier is restricted by the electron accumulation layer at the surface for all doping concentrations investigated. The band profile of the cap layer and QW become independent of N_D and, hence, the transition energy and electron-hole overlap do as well [see the left side of Fig. 3(c) and open circles in Fig. 3(d)].

3. Ga-face sample with thick cap

In Ga-face samples, the band-edge profile of the QW is superimposed by the field in the depletion layer beneath the surface, so that the transition energy and electron-hole overlap can be changed. Band profiles calculated for the sample with the 50-nm cap layer can be assigned to two cases [see the right side of Fig. 3(a)]. For the highest doping, the surface depletion layer is thinner than the cap and does not influence the QW, which remains in its intrinsic configuration, as already discussed above. The small difference in transition energy to the corresponding N-face case is caused by the asymmetry of the segregation profile. In the case of the two smaller doping concentrations, the QW is located

within the surface depletion layer, and the band edges are sufficiently far from the Fermi level so that the QW is not filled with carriers. The total potentials in the latter case are the superpositions of the respective QW potential (including the potential of the polarization charges), and the potential of the surface depletion layer, given by Eq. (13). The resulting net field inside the space-charge layer is approximately given by

$$F(z) = -\frac{eN_D}{\varepsilon\varepsilon_0}(\tilde{w}_s - z) + F_p\Theta_{\mathrm{QW}}(z). \tag{19}$$

The depletion width increased to

$$\tilde{w}_s = w_s\sqrt{1+\frac{eF_p d}{E_g}} \tag{20}$$

to keep the total potential drop at the GaN gap voltage E_g/e. Here w_s is the width of the surface depletion layer without a QW, given by Eq. (14).

Now we discuss the behavior of the total polarization field inside the QW when increasing the background doping density N_D. The surface depletion contribution to F (first term) has a sign opposite to that of the polarization contribution, thus reducing the transition redshift by counteracting the quantum-confined Stark effect. It vanishes for zero doping density, yielding the maximum field strength F_p, and increases like $\sim\sqrt{N_D}$ as long as the width $\tilde{w}_s$ of the surface depletion layer remains much larger than the thickness of the cap. The corresponding blueshift of the transition energies is depicted in Fig. 3(b). With a further increase of N_D, the depletion contribution reaches a maximum for $\tilde{w}_s = 2d_{cap}$, resulting in a saturation of the blueshift. Beyond this value the depletion contribution decreases and vanishes again for $\tilde{w}_s \to d_{cap}$, leaving behind the QW in its intrinsic configuration. However, a possibly related transition redshift does not occur. The dominant effect of the increasing hole confinement energy resulting from the steeper band edge alignment in the lower barrier yields a further blueshift of the transition energy, seen in Fig. 3(b). In addition, the screening effect from the successive filling of the electron groundstate subband with electrons from ionized donors contributes to a blueshift.

Although the screening mechanisms are different, the total blueshift obtained when increasing N_D from 5×10^{16} to 5×10^{18} cm^{-3} is approximately equal to the shift observed in case of the N-face QW with a 50-nm cap (80 and 150 meV for $x=0.1$ and 0.2, respectively). In the case of a Ga-face-grown QW with $x=0.05$ and a 50-nm cap layer, the interplay of the different screening mechanisms indeed results in a nonmonotonic behavior of the transition energy with increasing N_D, displayed in Fig. 4. For a QW with a smaller indium concentration, the filling of the electron subband appears at higher N_D due to the weaker confinement and the smaller unscreened field.

4. Ga-face sample with thin cap

The band profiles of a Ga-face sample with a 10-nm cap layer [left part of Fig. 3(a)] show some new effects with respect to the thick cap case. First, the net field in the QW vanishes for the highest donor concentration, in accordance with Eq. (19). A highly blueshifted transition could be expected. However, due to the segregated indium profile and the strong field in the depletion layer, the hole barrier is reduced to an extremely small value, and captured carriers will escape very quickly. If the characteristic escape time is much smaller than the radiative lifetime, no radiative emission from this QW can be expected. Therefore, no transition energies and overlap integrals are plotted for high doping and a small cap width.

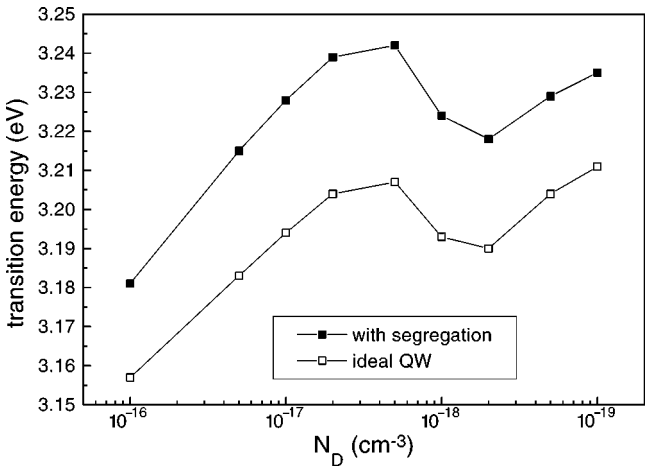

FIG. 4. Transition energy of a Ga-face-grown 3-nm $In_{0.05}Ga_{0.95}N$/GaN SQW with a 50-nm cap layer in dependence on a homogeneous background donor density with and without the consideration of indium surface segregation.

Second, for weakest doping, the valence-band maximum in the QW approaches the Fermi level, so that the hole ground state becomes occupied, forming a further inversion layer. The former surface depletion layer is now shifted into the sample, and a new thin surface depletion layer appears. Because of the relatively large density of states in the valence band, the band profile in the QW and the cap layer is nearly fixed by the requirement that the hole level is close to the Fermi energy. Thus the transition energy and electron-hole overlap remain nearly unchanged with increasing N_D, until the occupation of the hole subband becomes negligible.

The blueshifted transition energies and larger overlaps with respect to the thicker cap layer are consequences of the field distribution in the surface depletion layer. The thinner the cap layer, the higher is the depletion field and the more pronounced the counteraction of the quantum-confined Stark effect. Summarizing the case of a SQW in *n*-type GaN, we have found the following four qualitatively different situations.

(1) *Intrinsic configuration of the QW:* Sufficiently far from the surfaces, the polarization charges induce a thin electron accumulation layer at one interface in the QW and a rather thick space-charge region extending into the opposite barrier. With increasing N_D, the anticipated blueshift occurs.

(2) *QW close to a N-terminated surface:* The band profile and transition energy are independent of N_D.

(3) *QW in the surface depletion layer:* The transition energy is modified by the local electric field in the depletion layer and depends strongly on position and doping level.

(4) *QW close to a Ga-terminated surface:* In case of low doping concentrations, the band profile and transition energy are fixed by the occupation of the hole level in the QW. In

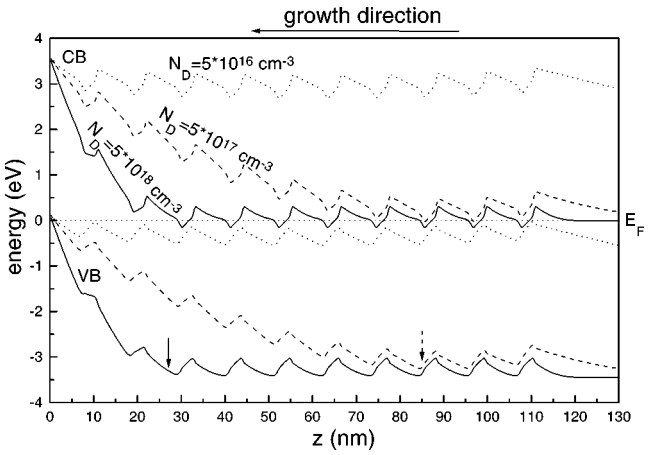

FIG. 5. Self-consistently calculated band-edge alignment of Ga-face-grown 3-nm (well)/8-nm (barrier) $In_{0.1}Ga_{0.9}N$/GaN 10MQW's for various background donor densities. The surface is at the origin of the abscissa. The effect of indium surface segregation is considered (see Sec. III).

the case of high doping ($N_D > 5\times10^{17}$ cm^{-3}) and low indium concentration ($x \leqslant 0.1$), carrier localization may be absent as a result of segregated interfaces and a high field in the surface depletion layer.

C. Multiple quantum well

In MQW structures, different QWs may experience different electric-field situations. In case of a Ga-face-grown MQW stack, the upper QW's reside within the surface depletion layer, whereas the lower QW's may already be below this region. This gives rise to a set of transition energies, and an extra inhomogeneous broadening of the optical transition feature. We discuss the self-consistent band profiles of a series of Ga-face-grown MQW stacks with different numbers of QW's, donor concentrations, and compositions. The well width is $d=3$ nm, the barriers and the cap layer are $d_b = d_{cap} = 8$ nm wide.

Figure 5 shows the result for a ten-period structure with $x=0.1$. In the case of medium and high doping, $N_D = 5\times10^{17}$ and 5×10^{18} cm^{-3}, respectively, the situation is as expected. The band profile in the depletion layer is approximately given by the superposition of the potential of the MQW and the space-charge potential. The resulting field strength $F(z)$ and the width $\tilde{w}_s$ of the depletion layer are still well described by Eqs. (19) and (20) when the total width of all depleted QW's is used for d. Below the depletion layer, the band profiles of the QW's are periodic. The interplay of segregation and a strong field in the surface depletion layer hinders the uppermost QW from confining carriers (see the solid lines in Fig. 5).

For very high doping, the profile of every period of this stack is equal to the intrinsic configuration of a SQW, discussed in Sec. III, and the fields of neighboring QW's are decoupled and given by Eq. (18). Decreasing the doping level, we arrive at a situation where the available space charge is limited by the MQW period, and the screening of the polarization field in the QW's is reduced in comparison with a SQW. Again using the approximations and notations of Sec. III, and demanding periodicity of the electrostatic potential, the electric-field profile within one period now becomes

$$F(z) = -\frac{eN_D}{\varepsilon\varepsilon_0}(z_i + L - z) + F_P\Theta_{\mathrm{QW}}(z) + F_0. \qquad (21)$$

Here z_i again denotes the position of the positively charged inverted interface of the respective QW, $\Theta_{\mathrm{QW}}(z)$ is again the domain function vanishing outside and is unity inside a QW, and $L = d_{QW} + d_b$ is the MQW period. The additional term $F_0 = eN_DL/2\varepsilon\varepsilon_0 - F_Pd/L$ is the residual field strength at the border $z = z_i + L$ to the adjacent QW. This field profile becomes independent of the doping for donor concentrations below σ_P/eL. Since the latter quantity is as high as 10^{19} cm^{-3}, the field profile of an undoped MQW is reached for donor concentrations of 10^{18} cm^{-3} and below.

An unexpected band profile is obtained in the low doping case, $N_D = 5\times10^{16}$ cm^{-3}. The valence-band-edge maxima of all QW's come close to the Fermi level, so that they are slightly populated with holes. This is the configuration of a MQW in *p*-type material. A closer inspection of the calculated charge and potential distributions shows (i) that the hole occupation in the QW's builds up at the expense of the surface inversion layer; (ii) that the occupation of the QW's is not strictly uniform but has maxima in the first and last QW; and (iii) that the depletion layer is shifted into the sample, now emerging beneath the deepest QW and having a width w_s given by Eq. (14).

Finally, to obtain a measure of how the distribution of optical transition energies and optical matrix elements affects a transition spectrum, we added the transitions of all contributing QW's in the form of phenomenologically broadened Gaussian curves, each positioned at the respective transition energy and equally weighed. In-plane inhomogeneities like compositional fluctuation and interface roughness are considered only implicitly by assuming a finite *x*-dependent linewidth for each transition (50 meV for $x=0.05$, 80 meV for $x=0.1$, and 100 meV for $x=0.2$), accounting for the tendency of larger linewidth in case of higher indium content.[39]

In Fig. 6, we see an additional broadening of the MQW transition spectra compared to the SQW transition, sensitively depending on the screening situation and the indium content. Especially for an indium concentration of $x \geqslant 0.1$ and a doping density of $N_D \geqslant 5\times10^{17}$ cm^{-3}, when the width of the depletion layer is in the same range like the thickness of the MQW, this broadening effect is strong and can also lead to a deformation or even splitting of the spectrum. High-energy features always stem from the last grown QW's directly under the sample surface. According to Eq. (15), there is the strongest depletion field, resulting in the strongest blueshift of the transition via counteracting the quantum-confined Stark shift. The relative heights of a multipeak spectrum, as well as the details of an emission line shape, depend sensitively on the relative contributions of each QW. These are in turn results of the mechanisms of absorption, relaxation, diffusion, transfer between the QW's, and radiative and nonradiative recombination, which are beyond the scope of this paper.

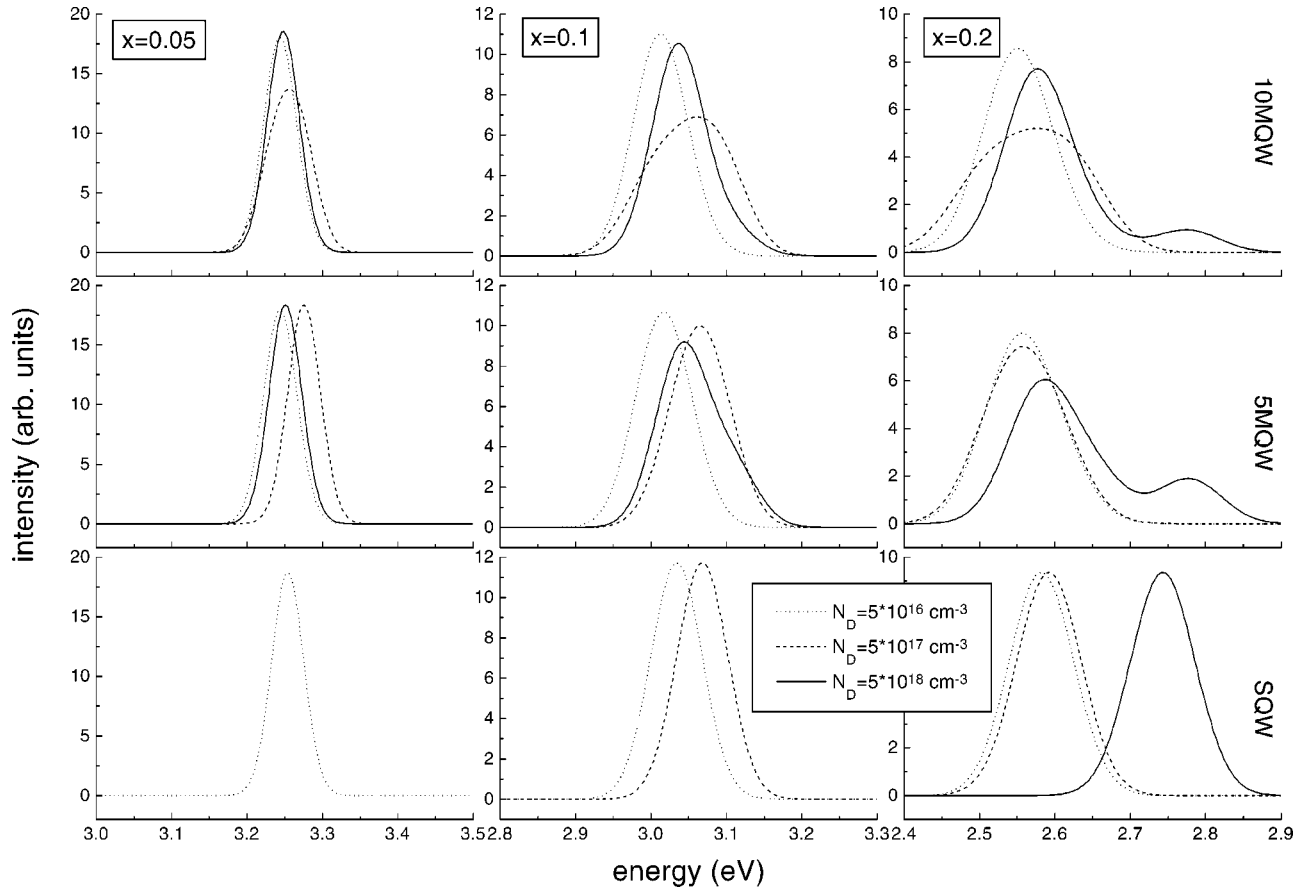

FIG. 6. Optical transition spectra of Ga-face-grown 3-nm (well)/8-nm (barrier) $In_xGa_{1-x}N/GaN$ SQW's, 5MQW's, and 10MQW's for various indium contents x and background donor densities N_D. The effect of indium surface segregation is considered (see Sec. III). In the case of a SQW, no line is drawn if carrier confinement cannot be expected due to a strong field in the depletion layer and low tunneling barriers. For $x=0.2$, all QW's contribute to the spectrum. For $x=0.1$, the last grown QW of the 5MQW and 10MQW does not contribute if the background density $N_D \geqslant 5\times10^{17}$ cm^{-3}. In the case of $x=0.05$, the same holds for the last two grown QW's, except for the 10MQW at $N_D=5\times10^{17}$ cm^{-3}, where only seven QW's contribute to the spectrum. Independent of the number of QW's contributing to the spectrum, the total intensities are normalized.

V. SUMMARY

We self-consistently calculated the band-edge alignments of (In,Ga)N/GaN SQW's and MQW's in an effective-mass model. On this basis, the influence of polarization charge screening and indium surface segregation on transition energies and electron-hole overlap integrals were investigated. We varied the background doping density, the thickness of the cap layer, the number of QW's, the indium content, and the polarity of the structure.

Indium segregation was shown to result in a blueshift of the emission energy compensating for up to one-third of the respective quantum-confined Stark shift. This blueshift is accompanied by a decrease of the electron-hole overlap compared to a rectangular indium profile, with the same integral indium content due to the asymmetry of the segregation lengths at the interfaces.

We showed that background doping influences the transition energy and overlap not only via screening of the polarization charge at material interfaces by mobile quantum-confined carriers, but also via ionized dopants in depletion layers. Therefore, the position of the QW in the sample with respect to an extended depletion layer—which was shown to exist in Ga-face-grown material with *n*-type doping—severely affects transition energy and electron-hole overlap. The interplay of the screening effects can even result in a nonmonotonic shift of the emission energy with increasing background donor density.

An optical transition spectrum of a Ga-face grown MQW can display shoulders or even a multipeak structure, depending sensitively on the background doping density and on the magnitude of inhomogeneous in-plane broadening. This effect is due to the spatial variation of the field strength in the surface depletion layer in Ga-face grown structures with *n*-type doping.

ACKNOWLEDGMENTS

We acknowledge the financial support of this work by the Deutsche Forschungsgemeinschaft and the stimulating discussions with P. Waltereit, A. Thamm, and O. Brandt from *Paul-Drude-Institut fuer Festkoerperelektronik*, Berlin.

*Electronic address: oliver.mayrock@physik.hu-berlin.de

[1] I-hsiu Ho and G. B. Stringfellow, Appl. Phys. Lett. **69**, 2701 (1996); T. Saito and Y. Arakawa, Phys. Rev. B **60**, 1701 (1999).

[2] See, e.g., A. Vertikov, A. V. Nurmikko, K. Doverspike, G. Bulman, and J. Edmond, Appl. Phys. Lett. **73**, 493 (1998); Y. Narukawa, Y. Kawakami, M. Funato, S. Fujita, S. Fujita, and S. Nakamura, *ibid.* **70**, 981 (1997); M. D. McCluskey, L. T. Romano, B. S. Krusor, D. P. Bour, N. M. Johnson, and S. Brennan, *ibid.* **72**, 1730 (1998); T. Sugahara, T. Sugahara, M. Hao, T. Wang, D. Nakagawa, Y. Naoi, K. Nishino, and S. Sakai, Jpn. J. Appl. Phys., Part 2 **37**, L1195 (1998); S. Sakai, T. Sugahara, S. Sakai, M. Lachab, R. S. Q. Fareed, S. Tottori, and T. Wang, Phys. Status Solidi B **216**, 273 (1999).

[3] C. Kisielowski, Z. Liliental-Weber, and S. Nakamura, Jpn. J. Appl. Phys., Part 1 **36**, 6932 (1997).

[4] See, e.g., Y. Narukawa, Y. Kawakami, S. Fujita, and S. Nakamura, Phys. Rev. B **59**, 10283 (1999); S. Chichiubu, T. Azuhata, T. Sota, and S. Nakamura, Appl. Phys. Lett. **69**, 4188 (1996); **70**, 2822 (1997); A. Satake, Y. Masumoto, T. Miyajima, T. Asatsuma, F. Nakamura, and M. Ikeda, Phys. Rev. B **57**, R2041 (1998); Y.-H. Cho, J. J. Song, S. Keller, U. K. Mishra, and S. P. DenBaars, Appl. Phys. Lett. **73**, 3181 (1998); K. P. O'Donnell, R. W. Martin, and P. G. Middleton, Phys. Rev. Lett. **82**, 237 (1999).

[5] F. Bernardini, V. Fiorentini, and D. Vanderbilt, Phys. Rev. B **56**, R10 024 (1997).

[6] K. Shimada, T. Sota, and K. Suzuki, J. Appl. Phys. **84**, 4951 (1998).

[7] T. Takeuchi, C. Wetzel, S. Yamaguchi, H. Sakai, H. Amano, I. Akasaki, Y. Kaneko, S. Nakagawa, Y. Yamaoka, and N. Yamada, Appl. Phys. Lett. **73**, 1691 (1998); T. Takeuchi, S. Sota, M. Katsuragawa, M. Komori, H. Takeuchi, and H. Amano, Jpn. J. Appl. Phys., Part 2 **36**, L382 (1997); **73**, 1691 (1998).

[8] A. Hangleiter, J. S. Im, H. Kollmer, S. Heppel, J. Off, and F. Scholz, MRS Internet J. Nitride Semicond. Res. **3**, 15 (1998); J. S. Im, H. Kollmer, J. Off, A. Sohmer, F. Scholz, and A. Hangleiter, Phys. Rev. B **57**, R9435 (1998).

[9] S. Chichibu, T. Sota, K. Wada, S. P. DenBaars, and S. Nakamura, MRS Internet J. Nitride Semicond. Res. **4S1**, G2.7 (1999); Appl. Phys. Lett. **73**, 2006 (1998).

[10] B. Monemar, J. P. Bergman, J. Dalfors, G. Pozina, B. E. Sernelius, P. O. Holtz, H. Amano, and I. Akasaki, MRS Internet J. Nitride Semicond. Res. **4**, 16 (1999).

[11] L.-H. Peng, C.-W. Chuang, and L.-H. Lou, Appl. Phys. Lett. **74**, 795 (1999).

[12] J. Dalfors, J. P. Bergman, P. O. Holtz, B. E. Sernelius, B. Monemar, H. Amano, and I. Akasaki, Appl. Phys. Lett. **74**, 3299 (1999).

[13] T. Wang, D. Nakagawa, M. Lachab, T. Sugahara, and S. Sakai, Appl. Phys. Lett. **74**, 3128 (1999).

[14] R. Cingolani, A. Botchkarev, H. Tang, H. Moroç, G. Traetta, G. Coli, M. Lomascolo, A. Di Carlo, F. Della Sala, and P. Lugli, Phys. Rev. B **61**, 2711 (2000).

[15] F. Della Sala, A. Di Carlo, P. Lugli, F. Bernardini, V. Fiorentini, R. Scholz, and J.-M. Jancu, Appl. Phys. Lett. **74**, 2002 (1999).

[16] V. Fiorentini, F. Bernardini, F. Della Sala, A. Di Carlo, and P. Lugli, Phys. Rev. B **60**, 8849 (1999).

[17] J. L. Sánchez-Rojas, J. A. Garrido, and E. Muñoz, Phys. Rev. B **61**, 2773 (2000).

[18] The difference between the free binding enthalpies of InN and GaN is about 10 kcal/mol, that is about 3 kcal/mol more than for the corresponding arsenides, where segregation is an already well investigated phenomenon. See *Semiconductors: Physics of Group IV Elements and III-V Compounds*, edited by O. Madelung, M. Schulz, and H. Weiss, Landolt-Börnstein, New Series, Group III, Vol. 17, Pt. a (Springer-Verlag, Berlin, 1982).

[19] J. E. Northrup, L. T. Romano, and J. Neugebauer, Appl. Phys. Lett. **74**, 2319 (1999).

[20] N. Duxbury, U. Bangert, P. Dawson, E. J. Trush, W. Van der Stricht, K. Jacobs, and I. Moerman, Appl. Phys. Lett. **76**, 1600 (2000).

[21] K. Muraki, S. Fukatsu, Y. Shiraki, and R. Ito, Appl. Phys. Lett. **61**, 557 (1992); J. Cryst. Growth **127**, 546 (1993); B. Lita, R. S. Goldman, J. D. Phillips, and P. K. Bhattacharya, Appl. Phys. Lett. **75**, 2797 (1999).

[22] J. Nagle, J. P. Landesman, M. Larive, C. Mottet, and P. Bois, J. Cryst. Growth **127**, 550 (1993).

[23] J.-M. Gerard and J.-Y. Marzin, Phys. Rev. B **45**, 6313 (1992).

[24] J. Massies, F. Turco, A. Saletes, and J. P. Contour, J. Cryst. Growth **80**, 307 (1987); Y. C. Kao, F. G. Celii, and H. Y. Liu, J. Vac. Sci. Technol. B **11**, 1023 (1993); M. D. Williams, T. H. Chiu, and F. G. Storz, *ibid.* **13**, 692 (1995).

[25] B. Koiller, R. B. Capaz, and H. Chacham, Phys. Rev. B **60**, 1787 (1999); L. Pfeiffer, K. W. West, H. L. Stormer, and K. W. Baldwin, Appl. Phys. Lett. **55**, 1888 (1989); T. Sajoto, M. Santos, J. J. Heremans, and K. W. Baldwin, *ibid.* **54**, 840 (1989); C. Gourdon, I. V. Mashkov, P. Lavallard, and R. Planel, Phys. Rev. B **57**, 3955 (1998).

[26] E. Berkowicz, D. Gershoni, G. Bahir, E. Lakin, D. Shilo, E. Zolotoyabko, A. C. Abare, S. P. DenBaars, and L. A. Coldren, Phys. Rev. B **61**, 10 994 (2000).

[27] R. F. Davis, Proc. IEEE **79**, 702 (1991); S. Strite and H. Morkoç, J. Vac. Sci. Technol. B **10**, 1237 (1992); *Properties of Group III Nitrides*, edited by J. H. Edgar (INSPEC, London, 1994).

[28] W. Shan, W. Walukiewicz, E. E. Haller, B. D. Little, J. J. Song, M. D. McCluskey, N. M. Johnson, Z. C. Feng, M. Schurman, and R. A. Stall, J. Appl. Phys. **84**, 4452 (1998); C. Wetzel, T. Takeuchi, S. Yamaguchi, H. Katoh, H. Amano, and I. Asaki, Appl. Phys. Lett. **73**, 1994 (1998); L. T. Romano, B. S. Krusor, M. D. McCluskey, D. P. Bour, and K. Nauka, *ibid.* **73**, 1757 (1998).

[29] K. Kim, W. R. L. Lambrecht, B. Segall, and M. van Schilfgaarde, Phys. Rev. B **56**, 7363 (1997); M. Suzuki, T. Uenoyama, and A. Yanase, *ibid.* **52**, 8132 (1995); J. A. Majewski, M. Städele, and P. Vogl, in *III-V Nitrides*, edited by T. Moustakas, B. Monemar, I. Akasaki, and F. Ponce, MRS Symposia Proceedings No. 449 (Material Research Society, Pittsburgh, 1997), p. 887.

[30] Y. C. Yeo, T. C. Chong, and M. F. Li, J. Appl. Phys. **83**, 1429 (1998); J. I. Pankove, S. Bloom, and G. Harbeke, RCA Rev. **36**, 163 (1975); R. D. Cunningham, R. W. Brander, N. D. Kbee, and D. K. Wickenden, J. Lumin. **5**, 21 (1972).

[31] C. G. Van de Walle and J. Neugebauer, Appl. Phys. Lett. **70**, 2577 (1997); S.-H. Wei and A. Zunger, *ibid.* **72**, 2011 (1998); C. Manz, M. Kunzer, H. Obloh, A. Ramakrishnan, and U. Kaufmann, *ibid.* **74**, 3993 (1999).

[32] A. F. Wright, J. Appl. Phys. **82**, 2833 (1997).

[33] E. S. Hellmann, MRS Internet J. Nitride Semicond. Res. **3**, 11 (1998); O. Ambacher, J. Smart, J. R. Shealy, N. G. Weimann, K. Chu, M. Murphy, R. Dimitrov, L. Wittmer, M. Stutzmann, W. Rieger, and J. Hilsenbeck, J. Appl. Phys. **85**, 3222 (1999).

[34] We used the freeware program *1D Poisson/Schrödinger* from http://www.nd.edu/~gsnider/.

[35] G. L. Snider, I.-H. Tan, and E. L. Hu, J. Appl. Phys. **68**, 2849 (1990); I.-H. Tan, G. L. Snider, L. D. Chang, and E. L. Hu, *ibid.* **68**, 4071 (1990).

[36] R. P. Leavitt and J. W. Little, Phys. Rev. B **42**, 11 774 (1990); P. Peyla, R. Romestain, Y. Merle d'Aubigné, G. Fishman, A. Wasiela, and H. Mariette, *ibid.* **52**, 12 026 (1995).

[37] S. M. Sze, *Physics of Semiconductor Devices*, 2nd ed. (Wiley, New York, 1981), Chap. 7.2.2., p. 372f.

[38] A. Rizzi and H. Lüth, Nuovo Cimento D **20**, 1039 (1998); V. M. Bermudez, J. Appl. Phys. **80**, 1190 (1996); S. S. Dhesi, C. B. Stagarescu, K. E. Smith, D. Doppalapudi, R. Singh, and T. Moustakas, Phys. Rev. B **56**, 10 271 (1997); O. Gfrörer, C. Gemmer, J. Off, J. S. Im, F. Scholz, and A. Hangleiter, Phys. Status Solidi B **216**, 405 (1999).

[39] K. P. O'Donnell, T. Breitkopf, H. Kalt, W. van der Stricht, I. Moerman, P. Demeester, and P. G. Middleton, Appl. Phys. Lett. **70**, 1843 (1997).